Controllable hydrothermal synthesis, growth mechanism, and properties of ZnO three-dimensional structures

Yangang Sun, Junqing Hu,* Na Wang, Rujia Zou, Jianghong Wu, Yuelin Song, Haihua Chen, Huihui Chen and Zhigang Chen

Received (in Victoria, Australia) 25th November 2009, Accepted 7th January 2010
First published as an Advance Article on the web 15th February 2010
DOI: 10.1039/b9nj00708c

A series of ZnO three-dimensional (3D) structures, including flower-like, star-like, sphere-like and sea urchin-like morphologies, have been fabricated by a hydrothermal method without any catalyst or template. The morphologies of these ZnO structures can be conveniently controlled, by selecting the reactants and controlling the experimental conditions, with excellent reproducibility, and a specific mechanism for the formation is proposed. The ZnO 3D structures have a strong emission peak at 405 nm, and several weak emission peaks at 452, 467, 493, 541 and 568 nm, and a high sensitivity and selectivity for gas sensing of ethanol.

1. Introduction

The development of rational approaches for well-defined three-dimensional (3D) interconnection of nanoscale building blocks into desired structures is a significant challenge in the realization of new functional materials and further applications.[1–3] Commonly, 3D architecture control has relied on anisotropic nanocrystal growth, template direction and the regulation of the growth rates of different crystal facets using a surfactant. This makes controlled growth of 3D inorganic nanostructures possible.[4,5] A wide range of one-dimensional (1D) ZnO nanostructures, including wires or rods, belts, and tubes,[6–12] has been prepared. So far, based on these 1D forms, much attention has been paid to the realization of 3D ZnO structures,[13–17] due to their unique properties[18] for novel applications, such as advanced catalysts and gas sensors. To date, several techniques have been used for the fabrication of ZnO 3D structures, including chemical vapor deposition (CVD), thermal evaporation, sonochemical methods, hydrothermal routes and pyrolysis techniques.[19–23] For example, Umar *et al.*[19] reported flower-shaped ZnO nanostructures on different orientations of silicon substrates, obtained using diethyl zinc and high purity oxygen (99.999%) gas as raw materials by the modified cyclic feeding chemical vapour deposition (CFCVD) technique. Zhang *et al.*[22] synthesized prickly sphere- and flower-like ZnO by decomposing $Zn(OH)_4^{2-}$ precursor in an aqueous solution, or $Zn(NH_3)_4^{2+}$ precursor in ethanol. Other groups reported on the synthesis of ZnO 3D nanostructures using a template with pre-deposited buffer layers[24] or different surfactants (additives), such as thiourea,[25] cetyltrimetylammonium bromide (CTAB),[26] hexamethylenetetramine (HMT),[27] ethylenediamine,[28] and so on. Moreover, Choppali and Gorman[23] obtained ZnO 3D structures with hexagonal flower-like morphologies by a polymeric precursor solution-based pyrolysis technique. However, previous efforts to synthesize ZnO 3D structures usually involved complex experimental procedures, complicated equipment, expensive substrates and surfactants, and (toxic) organic solutions to control their growth. It is a challenge to further fabricate ZnO 3D structures with low-cost, large scale, template-free methods, and without any surfactant or organic additive.

Herein, we present a one-step hydrothermal route to synthesizing ZnO 3D structures, including flower-like, star-like, sphere-like and sea urchin-like morphologies, which are simply tuned by changing the ratio of $Zn(NH_3)_4^{2+}$ precursor solution to water (solvent) and hydrothermal reaction temperature, and proposed the formation mechanism of ZnO 3D structures. Meanwhile, the gas sensing showed that flower-like ZnO structures had a high sensitivity and selectivity to ethanol. These ZnO products may have a potential application in sensors and other optoelectronic devices.

2. Experimental section

2.1 Synthesis

All reagents were analytically pure and used without further purification. The precursor solution was prepared by dissolving about 0.05 mol of $Zn(CH_3COO)_2{\cdot}2H_2O$, 0.1 mol of NaOH and 100 ml of $NH_3{\cdot}H_2O$ (25–28%) in deionized water with continuous stirring, and a white floccule firstly appeared and then completely dissolved. (By comparison, other Zn^{2+} sources, such as $ZnSO_4{\cdot}7H_2O$ and $ZnCl_2{\cdot}7H_2O$ were also investigated.) Subsequently, the as-formed solution was transferred into a volumetric flask, diluted to 250 ml with deionized water, and the precursor solution (Zn^{2+}: 0.2 mol L^{-1}) was obtained. In a typical procedure, an aqueous solution of precursor and deionized water were mixed in an equal volume and magnetically stirred for $\sim$10 min. Then, 32 ml of this mixture (Zn^{2+}: 0.1 mol L^{-1}) was transferred into a Teflon-lined stainless steel autoclave of 50 ml. Hydrothermal treatments were carried out at 180 °C for 12 h, and then the

State Key Laboratory for Modification of Chemical Fibers and Polymer Materials, College of Materials Science and Engineering, Donghua University, Shanghai 201620, China.
E-mail: hu.junqing@dhu.edu.cn

autoclave was cooled down to room temperature naturally. White precipitates were collected by centrifugation, and washed with deionized water and ethanol several times to remove impurities. Finally, the precipitates were dried in air at 60 °C for 5 h.

2.2 Characterization

The products were characterized with an X-ray diffractometer (XRD; Rigaku D/Max-2550 PC) equipped with Cu-Kα radiation, a scanning electron microscope (SEM; JSM-5600LV), and a transmission electron microscope (TEM; JEOL JEM 200CX 3000F) equipped with an X-ray energy dispersive spectrometer (EDS). The photoluminescence (PL) measurements were performed on a Perkin-Elmer luminescence spectrometer LS55 at room temperature using a Xe lamp with a wavelength of 325 nm as the light source.

2.3 Gas sensor fabrication and response test

The ZnO material was mixed with Terpineol and ground to form a paste. The paste was uniformly coated on an alumina tube with Au electrodes, followed by drying at 100 °C for 2 h, and annealing at 600 °C for about 2 h. Subsequently, a Ni–Cr heating wire was inserted. In order to improve the stability, the sensors were kept at the working temperature for several days. A stationary state gas distribution method was used for testing the gas response. The test was operated in a measuring system of HW-30A (Hanwei Electronics Co. Ltd., P. R. China). Detecting gases were mixed with air in a test chamber. The gas response of the sensor was defined as $R = R_a/R_g$ (reducing gases) or $R = R_g/R_a$ (oxidizing gases), where R_a and R_g were the resistance in air and test gas, respectively. The response or recovery time was expressed as the time taken for the sensor output to reach 90% of its saturation after applying or switching off the gas in a step function.

3. Results and discussion

3.1 Morphology and structure of ZnO 3D structures

All as-obtained powders show similar XRD patterns. A representative XRD pattern is shown in Fig. 1. The product, prepared with a volume ratio of $Zn(NH_3)_4^{2+}$ precursor solution to water of 1 : 1, at 180 °C for 12 h, can be indexed to a hexagonal ZnO phase with lattice constants of $a = 0.325$ and $c = 0.521$ nm (JCPDS card No. 36-1451). No characteristic peaks from precursor impurities, such as $Zn(CH_3COO)_2{\cdot}2H_2O$ and NaOH, are detected within experimental error. The sharp shape and narrow line widths of the diffraction peaks indicate that the ZnO material is highly crystalline.

A low-magnification SEM image (Fig. 2(a)) reveals that the products consist of radiolaria-like or flower-like ensembles composed of rod-like microstructures. The yield is as high as 60–70%, according to the amount of zinc acetate used. These flower-like microstructures are quite uniform, with average diameters of ~6–8 μm, as shown in Fig. 2(b). As further shown in the high magnification SEM image (Fig. 2(c)), the composed ZnO rods are regular hexagonal prisms with diameters of ~500 nm and lengths of several micrometres,

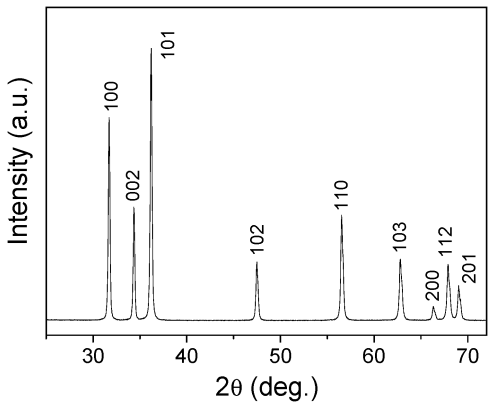

Fig. 1 XRD pattern of the product prepared with a volume ratio of $Zn(NH_3)_4^{2+}$ precursor solution to water of 1 : 1 at 180 °C for 12 h.

with well-defined, smooth and clean surfaces. The high-resolution TEM image is taken from an edge of a composed ZnO prismatic rod within the flower-like microstructures (Fig. 2(d)); it reveals that the rod is a single-crystal, and suggests that many single-crystal rods are self-assembled into ZnO 3D microstructures. Detailed analysis of the lattice fringes shows an interplanar spacing of 0.526 nm, which matches well with the distance of the (001) planes of a ZnO crystal resulting from lattice orientation perfections among the prismatic rods.[29,30] The rod axis direction is parallel to the [001] crystallographic orientation of a wurtzite ZnO crystal. This is a frequent growth orientation for hexagonal close-packed materials, which has been observed in many 1D ZnO forms.[31–33] This can be simply explained by the "low energy" argument; *i.e.*, the (0001) plane is the closest stacked in the wurtzite structures, and stacking along the [001] thus becomes energetically favorable.

3.2 The controllable synthesis of ZnO 3D structures

The morphologies of these ZnO 3D structures vary with the volume ratio of $Zn(NH_3)_4^{2+}$ precursor solution to water, from sea urchin-like to star-like, multi-petals-like and sphere-like flowers, assembled by the building blocks of hexagonal shapes, such as columns and cones, and prisms (Fig. 3). When the volume ratio of $Zn(NH_3)_4^{2+}$ precursor solution to water is

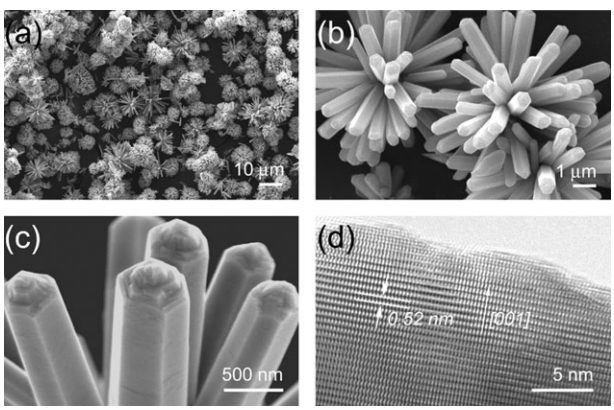

Fig. 2 (a)–(c) SEM images of the ZnO material synthesized using a volume ratio of $Zn(NH_3)_4^{2+}$ precursor solution to water of 1 : 1, at 180 °C for 12 h. (d) HRTEM image of as-synthesized ZnO product.

32 : 0 and the temperature reached 180 °C for 12 h, flower-like ZnO structures consisting of hexagonal columns with ~1 μm diameter and several micrometres length are obtained, as shown in Fig. 3(a). When the volume ratio is decreased to 1 : 3 and the temperature kept at 180 °C, the flower-like ZnO nanostructures consisting of hexagonal nanocones are prepared (Fig. 3(b)); when using $ZnSO_4$ as the Zn^{2+} source at 240 °C, star-like ZnO flower structures are fabricated (Fig. 3(c)). When the volume ratio is 1 : 7 and the temperature 180 °C, it can be seen that the flower-like ZnO consist of many nanorods with ~300–400 nm diameter and several micrometres length, which possess the typical tapering feature with the tips (Fig. 3(d)). While the reaction temperature is at 240 °C, sphere-like ZnO structures are formed (Fig. 3(e)). When the volume ratio is 1 : 15 and the temperature 180 °C, the ZnO products exhibit uniform urchin-like nanostructures composed of many ZnO nanorods with sharp tips (Fig. 3(f)); using $ZnCl_2$ as the Zn^{2+} source, beautiful flowers are observed (Fig. 3(g)). With further increasing the reaction temperature to 240 °C, the flower-like ZnO nanostructures are destroyed (Fig. 3(h)). So, large-scale ZnO crystals with a series of different flower-like morphologies are successfully fabricated by changing only the volume ratio of $Zn(NH_3)_4^{2+}$ precursor solution to water and reaction temperature; each flower-like ZnO 3D structure is composed of the ZnO cones, columns and prisms.

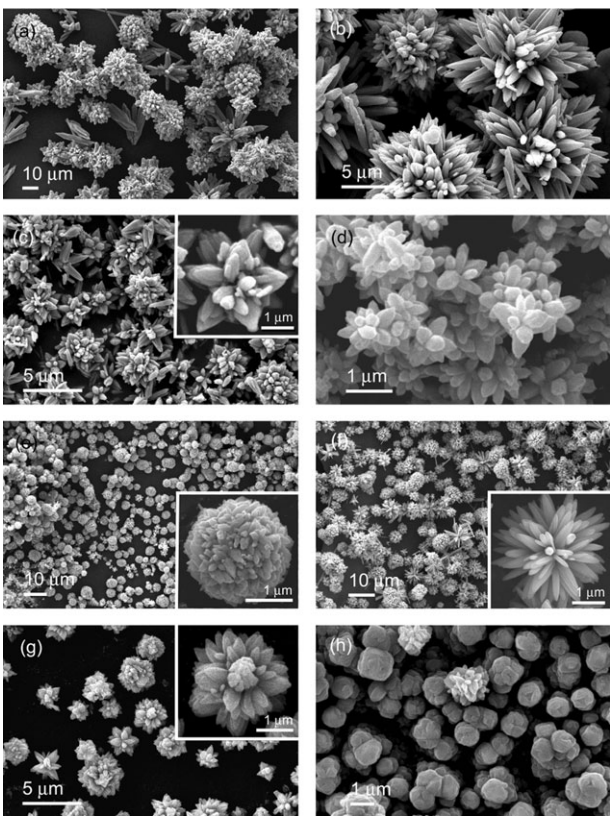

Fig. 3 SEM images of the ZnO 3D structures prepared at different volume ratio of Zn $(NH_3)_4^{2+}$ precursor solution to water: (a) 32 : 0, 180 °C; (b) 1 : 3, 180 °C; (c) 1 : 3, 240 °C, $ZnSO_4$ as Zn^{2+} source; (d) 1 : 7, 180 °C; (e) 1 : 7, 240 °C; (f) 1 : 15, 180 °C; (g) 1 : 15, 180 °C, $ZnCl_2$ as Zn^{2+} source; (h) 1 : 15, 240 °C.

3.3 Growth process

In the present case, we can fabricate ZnO particles by the direct decomposition of soluble $Zn(NH_3)_4^{2+}$ precursor under hydrothermal conditions, which follows the growth habit of ZnO crystals.[25] The crystal growth process involves two stages: nucleation and crystal growth.[22] External conditions may have tremendous effects on the morphology and size of a given crystal by participating in the nucleation and growth, in which many overall factors integrate to dominate the process. The real behavior of crystal growth in nanocrystallites may vary between fractal aggregation in the initial period and the subsequent diffusion process.

As is known to all, during the initial reaction period, reaction time affects merely the overall size of the aggregation instead of the morphology. With the reactant concentration decreasing gradually during a further extension of reaction time, the effect of diffusion processes which affect the overall size and the morphology have to be taken into account.[34]

From the reaction process point of view, the reactions for the formation of ZnO using the $Zn(NH_3)_4^{2+}$ precursor experience routes[22,35,36] according to the following reactions:

$$Zn^{2+} + 2OH^- \rightleftharpoons Zn(OH)_2\downarrow \quad (1)$$

$$Zn(OH)_2 + 4NH_3 \rightleftharpoons Zn(NH_3)^{2+}{}_4 + 2OH^- \quad (2)$$

$$Zn(OH)_2 \rightleftharpoons ZnO + H_2O \quad (3)$$

Obviously, at the beginning of this process, $Zn(OH)_2$ precipitates were obtained, evidenced by a white floccule appearing in our experiment. As the NH_3 solution was added, the $Zn(OH)_2$ precipitate began to dissolve, yielding a homogenous aqueous solution containing $Zn(NH_3)_4^{2+}$ ions.[37] The concentration of ammine complexes increased with an increase of the amount of ammonium. The supersaturation of the solid phases decreased with increasing NH_3, because the equilibrium in eqn (2) moved to the right, towards completely dissolving the above floccule. Thus, the solutions were stable and transparent with a large amount of the complexing agents. With the temperature increasing, the total concentration of NH_3 in the aqueous solution became lower due to a decrease of the NH_3 solubility in water—the equilibrium in eqn (2) moved to the left. Therefore, deposition and precipitation were observed,[38] where NH_3, as one of the byproducts, prevented the amalgamation of the nuclei[39] in the supersaturated solvents during the reaction process, thus leading to dispersed morphologies such as nanoparticles, prism-like or flower-like structures due to the different concentration growth units around the ZnO nuclei.[35,36]

In our experiments, the hydrothermal temperature plays a crucial role on the formation process of the ZnO 3D structures. So far, controllable experiments are performed by changing the temperature while maintaining other parameters. At room temperature or below 60 °C, no products are observed. At 80–100 °C, only ZnO nanocrystals can be obtained by keeping the reaction time for 20 min, as shown in Fig. 4(a). As the temperature is raised to 120 °C, the nanocrystals begin to aggregate into prism-like forms (Fig. 4(b)), indicating that the inherent anisotropic growth of ZnO crystals along the *c*-axis direction is favorable. With

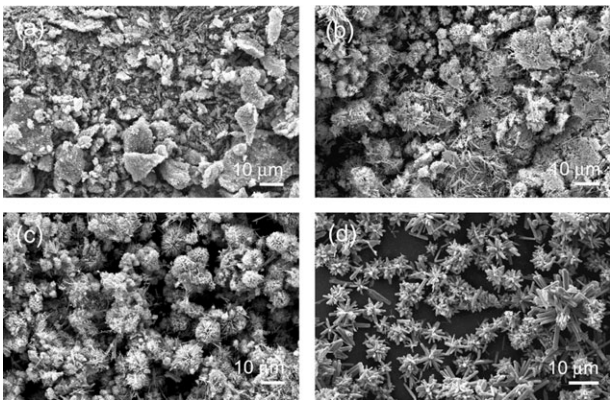

Fig. 4 SEM images of the conversion process from ZnO particles to rods and flower-like structures by controlling reaction temperature and time: (a) 100 °C, 20 min, (b) 120 °C, 20 min, (c) 180 °C, 20 min, (d) 120 °C, 12 h.

further increasing the temperature, as-obtained ZnO morphologies can be controlled from prism-like to flower-like structures. When the temperature is increased to 180 °C, ZnO flower-like structures are formed (Fig. 4(c)). Hence, the ZnO nanocrystals formed at different temperatures can grow further into ZnO nanowires, but their length and diameter are limited by the sizes of the initial ZnO nanocrystals. On the other hand, when the temperature is maintained at 120 or 180 °C and the reaction time is prolonged to 12 h, the nanocrystals and prisms begin to assemble into flower-like structures and the diameter of branched whiskers increase (Fig. 4(d) and 2(a)). This is due to the initial fast nucleation of ZnO nanocrystals, with crystal planes incompletely growing, and the traditional Ostwald ripening process controls the growth at the later stage.[40] So, the temperature is a crucial parameter for the formation of these flower-like structures, either from the initial growth nucleation stage or assembly stage.

3.4 Optical properties

We investigate the optical properties of ZnO flower-like microstructures using a combination of UV-vis and PL technologies. Fig. 5(a) shows the UV-vis spectra of ZnO flower-like microstructures with different sizes. The band gap energies (E_g) calculated on the basis of the corresponding absorption edges are 3.29 eV, which are comparable to the values of bulk ZnO. The PL properties of the as-prepared flower-like microstructures are measured using 372 nm as an excitation wavelength at room temperature. Fig. 5(b), curves a-d correspond to the ZnO microstructures (with the volume ratio of 1 : 1 and at 180 °C) obtained by different reaction times of 1, 6, 12 and 24 h, respectively. It is clear that the spectra consist of strong emission peaks located at 405 nm, and several weak emission peaks at 452, 467, 493, 541 and 568 nm. The near-UV emission at 405 nm agrees with the band gap of bulk ZnO (Gaussian peaks from 365–420 nm),[41–43] which comes from the recombination of free excitons.[44] The weak broad peaks at 452, 467 and 493 nm are attributed to the exciton transitions[45] and the presence of various point defects, either extrinsic[46] or intrinsic.[47] The green emissions at

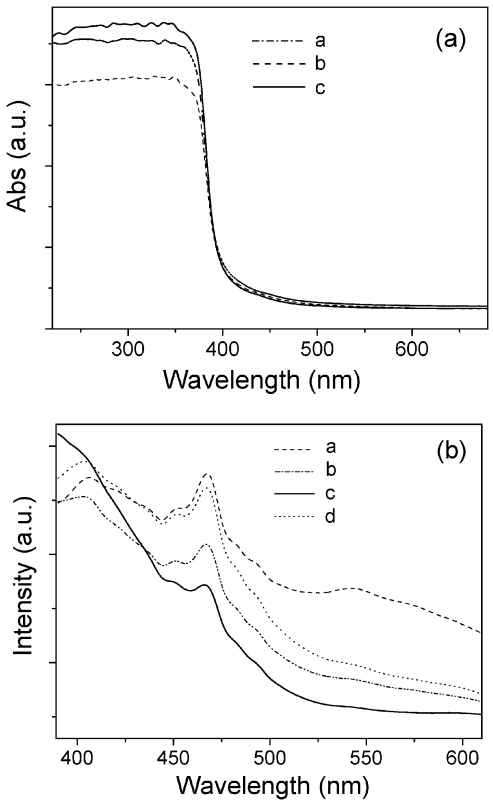

Fig. 5 (a) UV-vis absorption spectra, the volume ratio of $Zn(NH_3)_4^{2+}$ precursor solution to water: (a) 32 : 0, (b) 1 : 3, (c) 1 : 1. (b) Room temperature PL spectra of the ZnO flower-like microstructures: (a) 1 h, (b) 6 h, (c) 12 h, (d) 24 h.

541 and 568 nm are related to the singly ionized oxygen vacancy, and these emissions result from the recombination of a photogenerated hole with a singly ionized charge state of the specific defect.[48] The intensity of the visible emission peak in the spectra firstly becomes weak and then strong with increasing reaction time . It is related to the quantity of ionized oxygen vacancies and the level of lattice orientation perfections,[49] and luminescence properties can be controlled by changing the crystalline morphologies.

3.5 Gas sensing properties

The gas sensing properties of ZnO nanostructures have been widely investigated,[50,51] however, the influence of ZnO 3D structures on their gas sensing performance has scarcely been investigated. Here, we studied the ethanol gas sensing properties of ZnO flower-like morphologies. Eight typical reducing gases, CO, NO, H_2, NH_3, CH_3O, CH_3OH, CH_3COCH_3 and C_2H_5OH, and one typical oxidizing gas, NO_2, were selected as target gases to investigate the gas response under a heating voltage of 4 V (about 250 °C), where the concentration of all of the tested gases was 50 ppm. The gas sensor based on the ZnO flower-like structures showed good selectivity to ethanol, with little interference from other gases, whereas other gases did not show any response (Fig. 6). The response time and the recovery time of the ZnO flower-like structure-based sensors at the ethanol concentration of 50 ppm are shorter than 12 s (inset, Fig. 6). In comparison

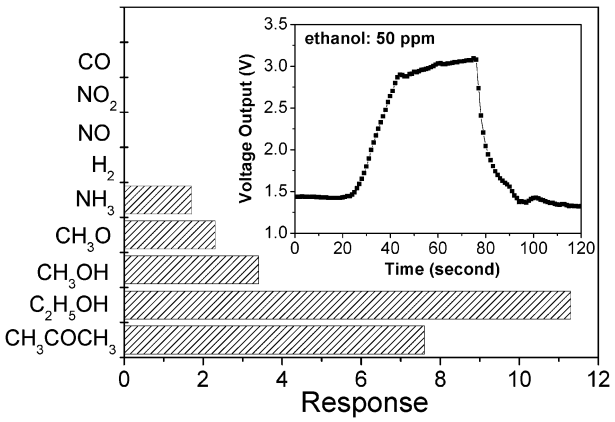

Fig. 6 Responses of the ZnO flower-like microstructures to various gases. The concentration of all gases was 50 ppm. Inset is the response curve of the sensor to 50 ppm ethanol.

with other ZnO morphologies for detecting ethanol,[52] the present ZnO flower-like microstructures exhibited excellent sensitivity and selectivity properties. The response enhancement of the gas sensing can be attributed to more active centers that are obtained from the enhanced oxygen vacancy defects on the junctions within the ZnO flower-like 3D structures.[53] The detailed response and selectivity mechanism need further investigation. It is expected that the ZnO flower-like morphology can be applied for monitoring ethanol in the environment and food, or even the drinking status of drivers.

4. Conclusion

A series of ZnO 3D structures, including flower-like, star-like, sphere-like and sea urchin-like morphologies, are fabricated by a simple hydrothermal method without any catalyst or template; each microstructure is assembled with many ZnO cones, columns and prisms. These morphologies can be conveniently controlled, by only selecting the reactants and controlling experimental conditions, with excellent reproducibility. Synthesis process studies of these ZnO 3D structures demonstrate that temperature is the crucial parameter for the formation of these flower-like structures either from the initial growth nucleation or assembly stage. Room-temperature PL spectra reveal that the ZnO 3D structures have a strong emission peak at 405 nm and several weak emission peaks at 452, 467, 493, 541 and 568 nm. The gas sensing shows that the ZnO flower-like structures have a high sensitivity and selectivity to ethanol. These ZnO products may have potentials as gas sensing material and other opto-electronic applications.

Acknowledgements

This work was financially supported by the National Natural Science Foundation of China (Grant No. 50872020 and 50902021), the Program for New Century Excellent Talents of the University in China, the "Pujiang" Program of Shanghai Education Commission (Grant No. 09P51400500), the "Dawn" Program of the Shanghai Education Commission (Grant No. 08SG32), the Shanghai Leading Academic Discipline Project (Grant No. B603), the "Chen Guang" project (Grant No. 09CG27) supported by the Shanghai Municipal Education Commission and Shanghai Education Development Foundation, the Program for the Specially Appointed Professor by Donghua University (Shanghai, P.R. China) and the Program of Introducing Talents of Discipline to Universities (No. 111-2-04).

References

1 Y. Huang, X. F. Duan, Q. Q. Wei and C. M. Lieber, *Science*, 2001, **291**, 630.
2 I. W. Hamley, *Angew. Chem., Int. Ed.*, 2003, **42**, 1692.
3 J. Q. Hu, Y. Bando and D. Golberg, *Small*, 2005, **1**, 95.
4 J. Tanori and M. P. Pileni, *Langmuir*, 1997, **13**, 639.
5 M. Li, H. Schnablegger and S. Mann, *Nature*, 1999, **402**, 393.
6 P. C. Chang, Z. Y. Fan, D. W. Wang, W. Y. Tseng, W. A. Chiou, J. Hong and J. G. Lu, *Chem. Mater.*, 2004, **16**, 5133.
7 L. Guo, Y. L. Ji, H. B. Xu, P. Simon and Z. Y. Wu, *J. Am. Chem. Soc.*, 2002, **124**, 14864.
8 B. Liu and H. C. Zeng, *J. Am. Chem. Soc.*, 2003, **125**, 4430.
9 Z. W. Pan, Z. R. Dai and Z. L. Wang, *Science*, 2001, **291**, 1947.
10 Y. B. Li, Y. Bando, T. Sato and K. Kurashima, *Appl. Phys. Lett.*, 2002, **81**, 144.
11 L. Vayssieres, K. Keis, A. Hagfeldt and S. Lindquist, *Chem. Mater.*, 2001, **13**, 4395.
12 J. Q. Hu, Q. Li, X. M. Meng, C. S. Lee and S. T. Lee, *Chem. Mater.*, 2003, **15**, 305.
13 B. Liu and H. C. Zeng, *J. Am. Chem. Soc.*, 2004, **126**, 16744.
14 P. Jiang, J. J. Zhou, H. F. Fang, C. Y. Wang, Z. L. Wang and S. S. Xie, *Adv. Funct. Mater.*, 2007, **17**, 1303.
15 H. Jiang, J. Q. Hu, F. Gu and C. Z. Li, *J. Phys. Chem. C*, 2008, **112**, 12138.
16 S. Cho, J. W. Jang, S. H. Jung, B. R. Lee, E. Oh and K. H. Lee, *Langmuir*, 2009, **25**, 3825.
17 L. P. Xu, Y. L. Hu, C. Pelligra, C. H. Chen, L. Jin, H. Huang, S. Sithambaram, M. Aindow, R. Joesten and S. L. Suib, *Chem. Mater.*, 2009, **21**, 2875.
18 P. X. Gao, J. L. Lee and Z. L. Wang, *J. Phys. Chem. C*, 2007, **111**, 13763.
19 A. Umar, S. Lee, Y. H. Im and Y. B. Hahn, *Nanotechnology*, 2005, **16**, 2462.
20 N. S. Ramgir, I. S. Mulla and V. K. Pillai, *J. Phys. Chem. B*, 2006, **110**, 3995.
21 S. Jung, E. Oh, K. Lee, Y. Yang, C. G. Park, W. Park and S. Jeong, *Cryst. Growth Des.*, 2008, **8**, 265.
22 J. Zhang, L. Sun, J. Yin, H. Su, C. Liao and C. Yan, *Chem. Mater.*, 2002, **14**, 4172.
23 U. Choppali and B. P. Gorman, *J. Am. Ceram. Soc.*, 2007, **90**, 433.
24 Y. J. Kim, J. Y. Yoo, B. H. Kwon, Y. J. Hong, C. H. Lee and G. C. Yi, *Nanotechnology*, 2008, **19**, 315202.
25 Z. Wang, X. F. Qian, J. Yin and Z. K. Zhu, *Langmuir*, 2004, **20**, 3441.
26 H. Zhang, D. Yang, Y. Ji, X. Ma, J. Xu and D. Que, *J. Phys. Chem. B*, 2004, **108**, 3955.
27 X. Gao, X. Li and W. Yu, *J. Phys. Chem. B*, 2005, **109**, 1155.
28 U. Pal and P. Santiago, *J. Phys. Chem. B*, 2005, **109**, 15317.
29 J. F. Banfield, S. A. Welch, H. Z. Zhang, T. T. Ebert and R. L. Penn, *Science*, 2000, **289**, 751.
30 R. L. Penn and J. F. Banfield, *Science*, 1998, **281**, 969.
31 J. Q. Hu, Q. Li, N. B. Wong, C. S. Lee and S. T. Lee, *Chem. Mater.*, 2002, **14**, 1216.
32 L. E. Greene, B. D. Yuhas, M. Law, D. Zitoun and P. D. Yang, *Inorg. Chem.*, 2006, **45**, 7535.
33 X. Liao and X. Zhang, *J. Phys. Chem. C*, 2007, **111**, 9081.
34 B. M. Wen, Y. Z. Huang and J. J. Boland, *J. Phys. Chem. C*, 2008, **112**, 106.
35 N. Saito, H. Haneda, W. S. Seo and K. Koumoto, *Langmuir*, 2001, **17**, 1461.
36 C. L. Wu, X. L. Qiao, L. L. Luo and H. J. Li, *Mater. Res. Bull.*, 2008, **43**, 1883.

37 H. Zhang, D. R. Yang, X. Y. Ma, Y. J. Ji, J. Xu and D. L. Que, *Nanotechnology*, 2004, **15**, 622.
38 S. Yamabi and H. Imai, *J. Mater. Chem.*, 2002, **12**, 3773.
39 J. Zhang, L. Sun, C. Liao and C. Yan, *Chem. Commun.*, 2002, 262.
40 H. Qian, S. Yu, J. Gong, L. Luo and L. Wen, *Cryst. Growth Des.*, 2005, **5**, 935.
41 S. Monticone, R. Tufen and A. V. Kanaev, *J. Phys. Chem. B*, 1998, **102**, 2854.
42 E. M. Wong and P. C. Searson, *Appl. Phys. Lett.*, 1999, **74**, 2939.
43 H. Jiang, J. Q. Hu, F. Gu and C. Z. Li, *Nanotechnology*, 2009, **20**, 055706.
44 V. Srikant and D. R. Clarke, *J. Appl. Phys.*, 1998, **83**, 5447.
45 B. J. Jin, S. H. Bae, S. Y. Lee and S. Im, *Mater. Sci. Eng., B*, 2000, **71**, 301.
46 R. Dingle, *Phys. Rev. Lett.*, 1969, **23**, 579.
47 K. Vanheusden, W. L. Warren, C. H. Seager, D. R. Tallant, J. A. Voigt and B. E. Ganade, *J. Appl. Phys.*, 1996, **79**, 7983.
48 Y. Li, G. S. Cheng and L. D. Zhang, *J. Mater. Res.*, 1999, **15**, 2305.
49 Y. Masuda, N. Kinoshita, F. Sato and K. Koumoto, *Cryst. Growth Des.*, 2006, **6**, 75.
50 L. Liao, H. B. Lu, J. C. Li, H. He, D. F. Wang, D. J. Fu, C. Liu and W. F. Zhang, *J. Phys. Chem. C*, 2007, **111**, 1900.
51 G. Kwak and K. J. Yong, *J. Phys. Chem. C*, 2008, **112**, 3036.
52 Y. Zhang, J. Xu, Q. Xiang, H. Li, Q. Pan and P. Xu, *J. Phys. Chem. C*, 2009, **113**, 3430.
53 D. H. Zhang, Z. Q. Liu, C. Li, T. Tang, X. L. Liu, S. Han, B. Lei and C. W. Zhou, *Nano Lett.*, 2004, **4**, 1919.